IOPscience iopscience.iop.org

Home Search Collections Journals About Contact us My IOPscience

Fabrication of complex curved three-dimensional silicon microstructures using ion irradiation

This article has been downloaded from IOPscience. Please scroll down to see the full text article.

2012 J. Micromech. Microeng. 22 015015

(http://iopscience.iop.org/0960-1317/22/1/015015)

View the table of contents for this issue, or go to the journal homepage for more

Download details:
IP Address: 137.132.3.9
The article was downloaded on 11/01/2012 at 07:00

Please note that terms and conditions apply.

IOP Publishing Journal of Micromechanics and Microengineering
J. Micromech. Microeng. **22** (2012) 015015 (9pp) doi:10.1088/0960-1317/22/1/015015

Fabrication of complex curved three-dimensional silicon microstructures using ion irradiation

S Azimi, M B H Breese, Z Y Dang, Y Yan, Y S Ow and A A Bettiol

Department of Physics, Centre for Ion Beam Applications (CIBA), National University of Singapore, Singapore 117542

Received 27 September 2011, in final form 8 November 2011
Published 23 December 2011
Online at stacks.iop.org/JMM/22/015015

Abstract
We have developed a process to fabricate arbitrary-shaped, three-dimensional microstructures in 0.4 Ω cm p-type silicon using focused high-energy proton beam irradiation, followed by electrochemical anodization. This has enabled us to produce free-standing complex microstructures such as arrays or long wires, grids, wheels, vertically stacked wires and wires which can be controllably bent upward and downward in the vertical plane. The two most important factors which determine the wire cross-section dimensions and depth are the irradiation ion fluence and energy. We can controllably vary the width of wires from 1 to 5 μm by varying the fluence of 1 MeV protons and the depth of wires from 2 to 15 μm by varying the proton energy. By using a combination of multiple energy proton irradiation over a range of 200–1000 keV, and gray-scale masks, different ion penetration depths and multilevel free-standing three-dimensional silicon structures can be obtained in a single etch step.

(Some figures may appear in colour only in the online journal)

1. Introduction

There is a wide spectrum of scientific and technological disciplines in which precisely machined, three-dimensional (3D) micro- and nano-scale structures are required in silicon-based materials. For example, in silicon photonics near- and mid-infrared regions [1–4], conventional silicon waveguide structures are fabricated in SOI (silicon-on-insulator) wafers, which do not readily allow 3D waveguides between circuitry at different depths within the wafer. Therefore, the ability to controllably fabricate 3D lines and wires is highly desirable for coupling between circuits at different depths, and allows better 3D integration and packing density of photonic devices with each other and with microelectronic components. It would also allow new options for the design and fabrication of high-aspect ratio, multilevel microstructures in silicon for optoelectronic and in micro- and nano-electromechanical systems [5–7] and in fabricating photonic crystals [8].

Various techniques have been described in the literature for 3D silicon microfabrication. Such structures are most commonly fabricated either by surface machining, focused ion beam (FIB), multiple lithography, gray-scale lithography, reactive ion etching (RIE) lag-based methods or controlled under-etch/recovery in the deep reactive ion etching (DRIE) process. Generally, silicon–silicon dioxide layers on a silicon substrate are used in surface machining [9]. The top layer is selectively etched by the defined mask pattern and the sacrificial silicon oxide layer can be removed for undercutting silicon structures. FIB can also be used for silicon surface milling by irradiating a surface with a focused gallium ion beam and by utilizing sputtering, etching and ion beam-induced deposition [10]. In gray-scale lithography, the gradient height profiles in a photoresist mask are transferred to the silicon substrate using anisotropic RIE [11]. Deliberate modulation of the mask pattern openings defines the etch depth variation in the RIE lag-based method [12, 13]. Controlling the process parameters such as power density, gas flows and timings in the sequential DRIE process will also result in desired deep vertical etching with controlled under-etching and recovery, yielding 3D features on a silicon substrate [14]. Complex 3D structures can be constructed by combination of machining different parts and assembly processes [15]. These techniques, however, require multiple or unconventional

 © 2012 IOP Publishing Ltd Printed in the UK & the USA

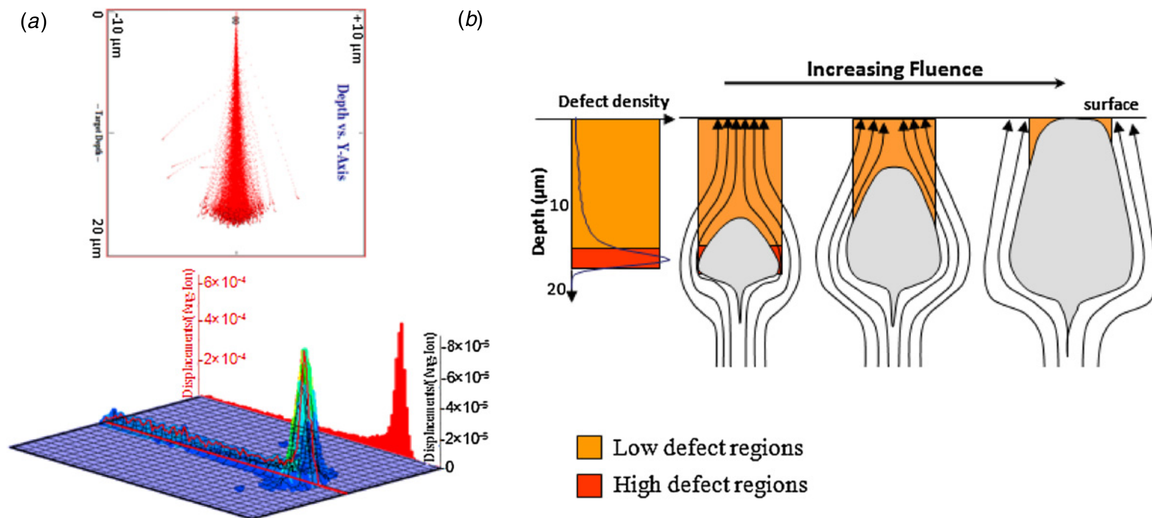

Figure 1. (*a*) SRIM simulation of (top) trajectories versus depth and (bottom) defect distribution for 1 MeV protons in silicon. (*b*) Schematic showing the damage profile and deflected hole current around high defect region during anodization. At suitable fluences, the holes bend round the high defect region and flow through the lower defect region.

processes and show limitations in fabrication of complex 3D geometries.

We have developed a technique using ion beam irradiation capable of fabricating arbitrary, curved multilevel 3D structures in bulk silicon in a single etch step. Previously we have demonstrated micromachining of multilevel surface-relief silicon structures and modified photoluminescence using damage deliberately introduced by focused, high-energy ion beams [16]. In this process, high-energy ions, typically protons or helium, with energies of 250 keV to 2 MeV, are focused to a beam spot of a few hundred nanometers in a nuclear microprobe [17] for direct proton beam writing on p-type silicon.

Ion irradiation causes crystalline damage to the silicon, mainly in the form of vacancy-interstitial pairs, i.e. Frenkel defects [18–21]. These can be completely recovered by thermal annealing after the fabrication process. Hence, the low fluence used for this micromachining process has no effect on the optical properties of silicon. While agglomeration of the ions used for irradiation may occur, the fluence is very low ($\sim 10^{14}$ cm^{-2}) compared with, for example, smart-cut silicon (10^{16}–10^{17} cm^{-2}), and only within the patterned areas, so we do not consider that this limits the performance of the photonic structures fabricated using this approach. Similarly, the low fluence ensures that the silicon lattice is only lightly damaged, the fluence being several orders of magnitude lower than that at which noticeable amorphization occurs. The use of this ion irradiation-based process to fabricate low loss waveguides has been verified by measuring the propagation losses of micrometer width waveguides made in this manner, with losses of ∼1 dB cm^{-1} obtained [22, 23].

The ion-induced defects locally reduce the free carrier density, hence increasing the resistivity of the irradiated silicon regions, reducing the rate of porous silicon (PSi) formation during subsequent electrochemical anodization. Higher fluence irradiation can act as an etch stop for PSi formation [24]. The underlying multilevel silicon structure may be easily revealed by removing the PSi with potassium hydroxide (KOH).

2. Experimental aspects

In this paper, we describe further development of this process for micromachining of complex, 3D free-standing silicon structures in 0.4 Ω cm p-type silicon, chosen as suitable material for fabricating components for silicon photonics, whereas low carrier density is required to reduce propagation loss by scattering from free carriers [1]. We make use of the fact that high-energy protons create significantly more localized defects at their end of range than close to the surface. Figure 1(*a*) shows SRIM (stopping and range of ions in matter) [21] simulation of the trajectories of 1 MeV protons in silicon. The beam tends to remain well collimated, with little lateral scattering until the ions slow down close to their end of range. 1 MeV protons have a range of ∼16 μm in silicon, with a FWHM (full-width-at-half-maximum) of the lateral distribution of ∼2 μm. The defect generation rate is more than ten times higher at the end of range compared to the trajectory closer to the surface [25]. By controlling the fluence within each point of an irradiated area, the resistivity can be controlled and increased locally for selective PSi formation [25], as shown in figure 1(*b*). Wafers are then electrochemically anodized in an electrolyte containing HF (48%):water:ethanol (1:1:2) for 12 min with a current density of 60 mA cm^{-2}, giving an etch depth of about 27 μm. During the electrochemical process, the flow of electrical holes from the back surface bends around the high defect regions to the front surface. As a result, PSi forms around these regions, leaving the core region intact, with the size and depth depending on the proton fluence and energy.

The ion energy, fluence and beam size can all influence the core size. Figure 2 shows SRIM results for the (a) proton range in silicon and (b) defect distribution for 10 000 simulated protons in each case versus lateral position across the end-of-range core region for different proton energies, typical of those used in our recent studies. Use of higher energies allows deeper

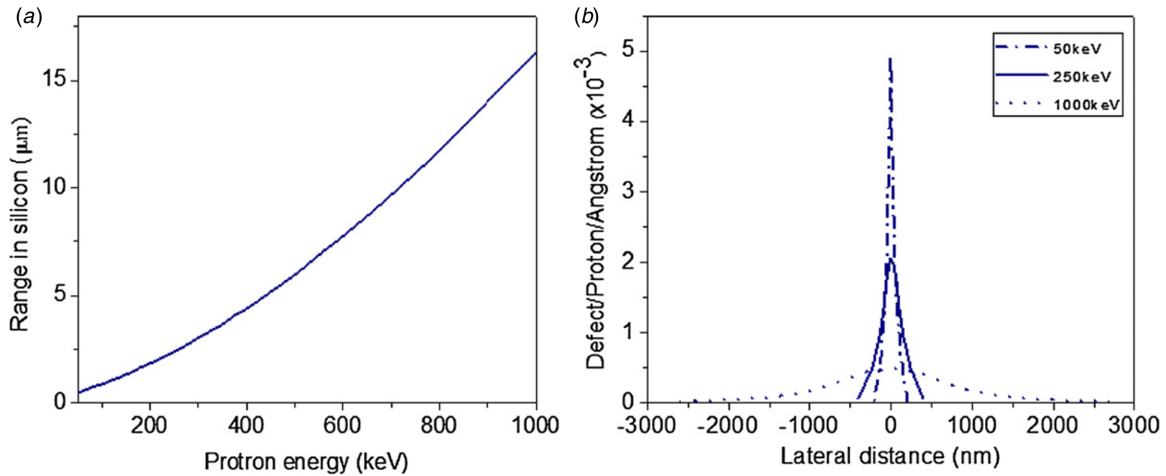

Figure 2. (*a*) Plot of proton range versus energy in silicon. (*b*) Plot of defect density versus lateral distance across the end-of-range core for different proton energies in silicon.

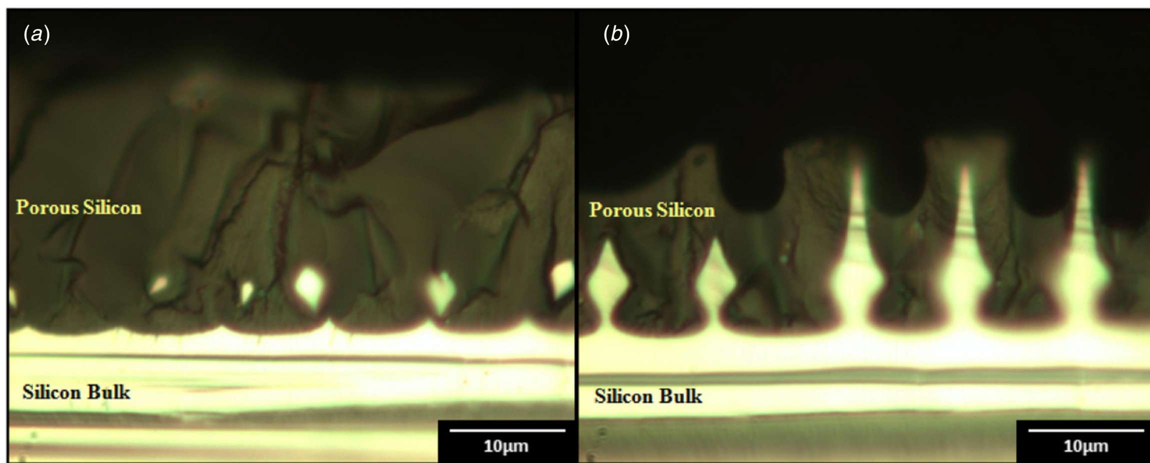

Figure 3. Optical images showing wire cross sections buried in PSi after irradiation with 1 MeV protons with a line fluence of (*a*) 1.5×10^{10}, 3×10^{10}, (*b*) 6×10^{10} and 1.2×10^{11} cm^{-1}.

irradiation, with core formed further beneath the surface. The further ions travel through matter, the more they are scattered in small-angle collisions with the sample electrons. Hence, the larger scattering at higher proton energies results in defects distributed over a wider distance away from the beam axis, so larger core sizes are expected at higher energies.

The standard unit to quantify the number of ions used for irradiation is the fluence, defined as the number of ions incident upon a given surface area, in units of ions cm^{-2}. This definition is ideal for irradiating large areas where the effects of irradiation are laterally uniform and the defect depth distribution may be calculated using codes such as SRIM. Indeed we have used this approach to model the ion-induced defect density as a function of depth and used this to model the effects of ion fluence on anodization of large areas where the lateral extent of the irradiated area was bigger than the end-of-range scattering [25]. However, the present study considers an unusual irradiation regime in which ion scattering results in a lateral extent of the defects across the end-of-range region which is significantly larger than the irradiated line width on the wafer surface (figure 1(*a*)). The fluence is not the most relevant factor in determining the core size, since as the surface width of an irradiated line becomes similar to, or less than, the end-of-range lateral scattering, the peak defect density decreases even though the fluence remains the same. Here we define a more useful parameter for this work, which is the line fluence, given by the number of ions used for irradiating a line of zero width per centimeter of line length. This definition is independent of the irradiated line width on the surface and it simplifies the experimental aspects of fabricating small cores since the only parameter is the total number of ions used and the line length.

Figures 3(*a*) and (*b*) show cross-section optical images of cores produced by irradiation with increasing line fluences of 1 MeV protons using a beam focused to a spot size of 200 nm. By increasing the line fluence from 1.5×10^{10} to 1.2×10^{11} cm^{-1}, the width of the core increases from about 1 to 5 μm, respectively. At the same time, the core cross section elongates, as shown in figure 3(*b*), as the defect density all along the irradiation path increases to the level where it significantly deflects the flow of hole current.

Schematics of the three irradiation processes used in this paper are shown in columns (i)–(iii) in figure 4. Supporting walls for the final free-standing structures are defined using 2 MeV protons (range of $\sim$48 μm) with a high line fluence of 1.2×10^{12} cm^{-1}, which is enough to completely stop

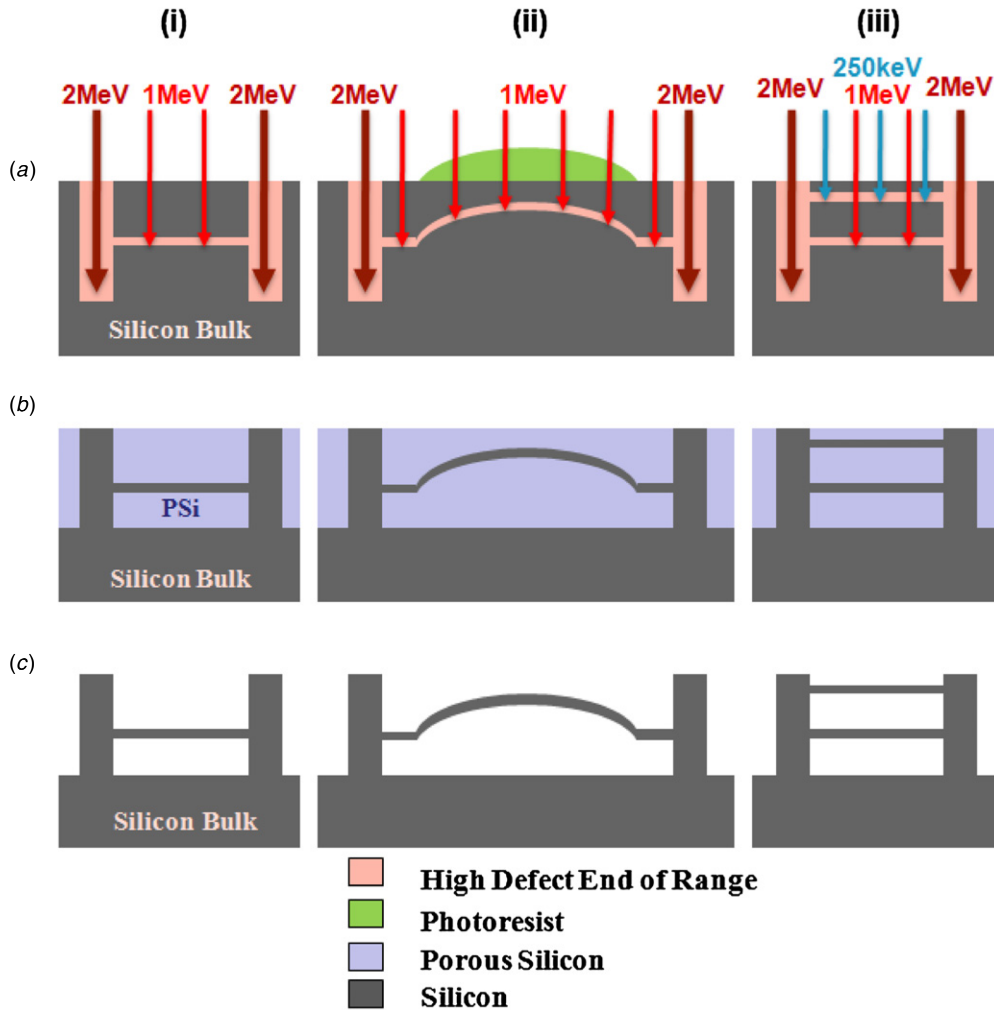

Figure 4. Schematics of the processes involved in fabricating (i) flat, (ii) curved and (iii) multilevel free-standing 3D wires using (*a*) 1 MeV and 250 keV proton irradiation for wires and 2 MeV protons with a high line fluence for supporting walls, (*b*) anodization to produce PSi around the cores and (*c*) removal of the PSi leaving a free-standing structure.

anodization at the irradiated regions. In process (i), single energy (1 MeV) proton irradiation with a low line fluence of 1×10^{10} cm^{-1} is used to create end-of-range cores at a single depth. Focused beam irradiation may be of any shape, such as lines or circles. During anodization in figure 4(*b*), current flows through those regions above and below the end-of-range core region, resulting in PSi formation. No current flows through the core or the supports. Finally, very dilute KOH solution is used to release the free-standing 3D silicon structures, figure 4(*c*).

3. Results and discussions

3.1 Single–level 3D wires

We have fabricated arrays of long wires using the approach in figure 4(*i*) by irradiating lines of 500 μm length with 1 MeV protons, figures 5(*a*) and (*b*). A long supporting wall midway along their length and shorter ones at different spacings were included with the aim of studying how long such free-standing wires could be made. None of the wires have broken, showing that free-standing wires of diameter about 1 μm can be produced over 200 μm long. The higher magnification SEMs in figures 5(*a*) and (*b*) respectively show the end of the wires suspended above the etched silicon surface and details of where the wire joins the support. Note a widening of the wire where it meets the support and the slight protrusion at the support in the vertical direction, both above and below the wire, indicated by arrows. Above the wire, the protrusion is attributed to the lower defect density formed above the core by the 1 MeV proton irradiation. This is not high enough to stop anodization above the wire, but enough to produce a slight decrease in etch rate at the support wall where the defect density is already high. The protrusion below the wire reflects the depth beneath the core of about 3 μm at which the hole current flowing to the surface starts to bend around the wire, reducing the current density at the supporting wall. In the higher magnification SEM in figure 5(*a*), the protrusion of the underlying silicon surface reflects the reduced etch rate associated with the core formation.

3.2 Complex 3D structures

Using proton beam writing for selective irradiation gives the ability to directly fabricate arbitrary patterns, not necessarily

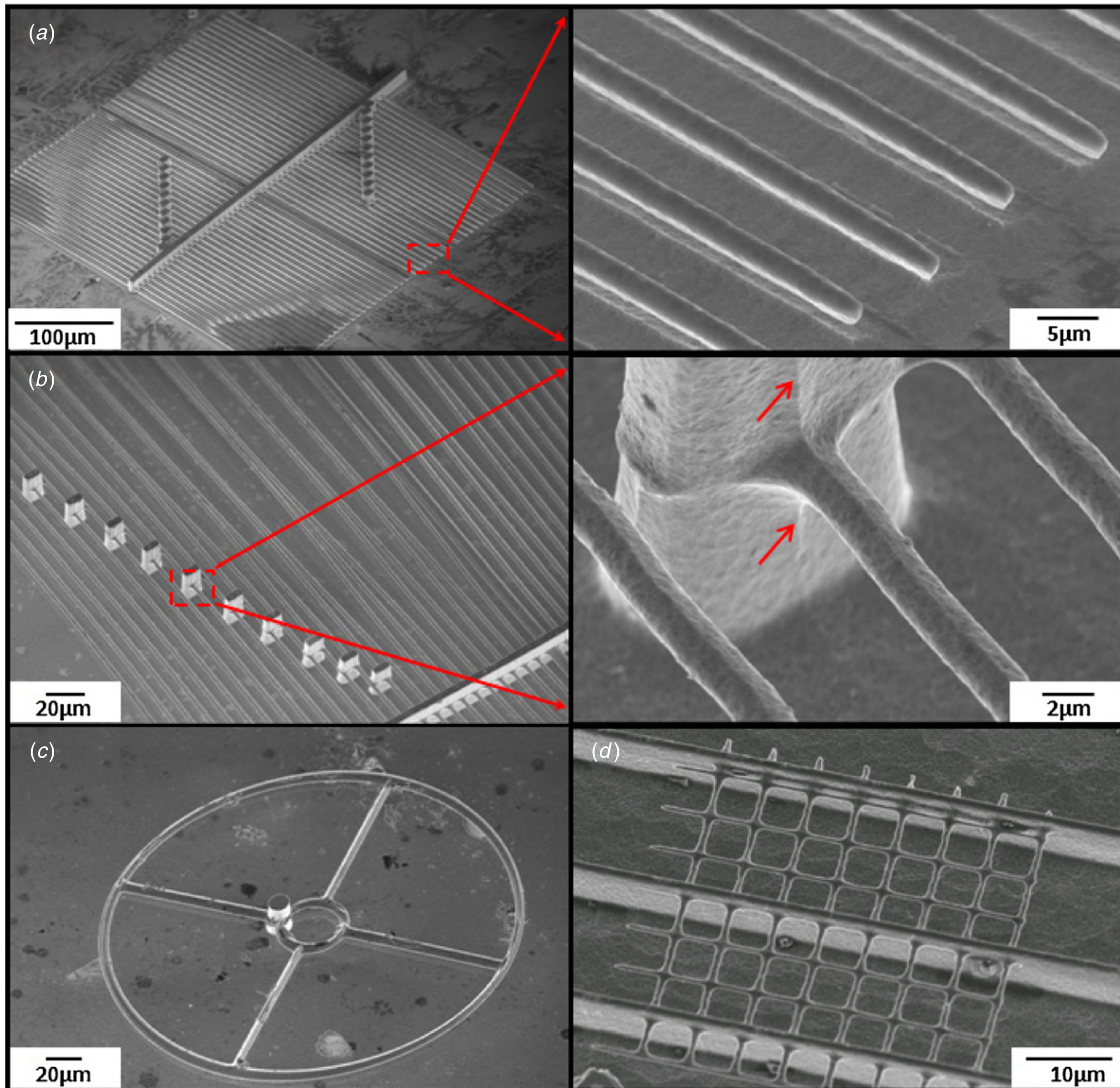

Figure 5. SEM images of 3D machined arrays of free-standing cores forming various shapes, supported by heavily irradiated silicon walls. (*a*), (*b*) Wires and their close-up views. (*c*) 3D-machined wheel with a pillar for support. (*d*) Grid formed by irradiation with 250 keV protons. The tilt angle of all tilted SEM images are $\sim 30^{\circ}$.

just lines as described above. Figure 5(*c*) shows a simple free-standing wheel supported by a pillar, fabricated as an example to show the further capability of this technique for fabricating more complicated structures. The axle was deliberately offset from the center of the wheel so that the wheel was held in place, rather than being free to rotate, so that it could be more easily recorded as a free-standing structure. Figure 5(*d*) shows a grid structure, formed using the same process except using 250 keV protons (range 2.6 μm, FWHM 460 nm), line fluence of 1×10^{10} cm^{-1} to produce the end-of-range cores as a grid structure, again supported by higher energy irradiations. Since the FWHM beam spread at the end of range is considerably smaller than for 1 MeV protons, a smaller wire cross section of 800 nm is produced.

3.3 Vertically curved 3D wires

3D silicon microstructures which are curved in the vertical plane can be similarly micromachined, with the addition of a thin, patterned gray-scale resist mask with sloping edges, see process (ii) in figure 4. The gray-scale mask was fabricated in SU-8 resist using a two-photon lithography (TPL) fabrication system. The ultrafast pulses, with a centre wavelength of 800 nm and pulse width of approximately 150 fs, are generated by a mode-locked Ti:sapphire oscillator and can selectively polymerize a small focal volume inside the photoresist. By scanning the stage in all three dimensions, an arbitrary 3D polymer structure can be fabricated, see figure 6(*d*) (inset). For this purpose, the 3D design of the mask is first sliced in AutoCAD into layers of 2D bitmaps, which are then patterned by the laser, with different layers at different height levels. The distance between each layer is set at 0.6 μm to avoid the 'step' shape sidewall profile. Although the 800 nm wavelength is far from the absorbance peak of SU-8 which is located near 400 nm, at the tiny focal volume, a peak power as high as 150 KW is achieved, allowing the SU-8 to be polymerized by simultaneously absorbing two photons. The gray-scale mask is ready after laser irradiation which is followed by postbaking

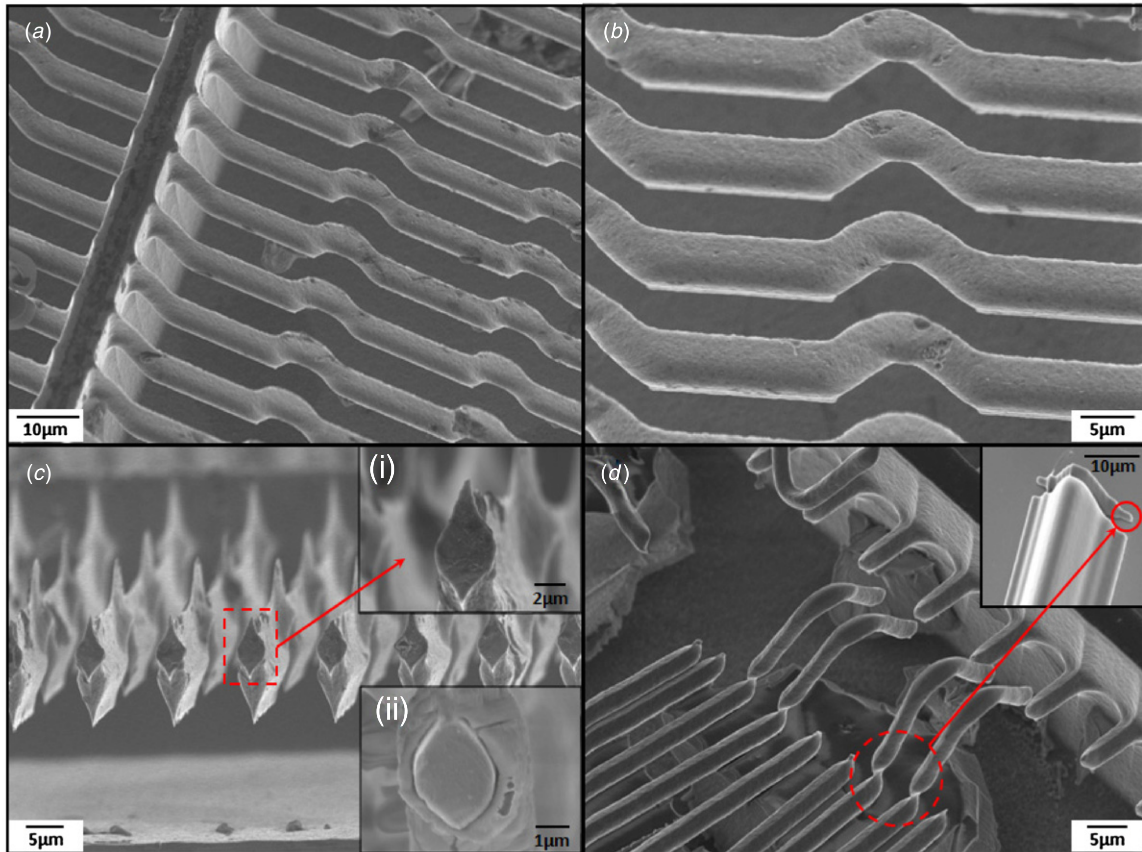

Figure 6. SEM images of micromachined (*a*),(*b*) curved 3D wires and (*c*) SEM cross section and close-up view of one of the wires (i) before and (ii) after oxidation. (*d*) An example failure in fabrication of curved 3D wires due to the step at the edge of the resist pattern. The inset shows the resist line used on the sample to modify the end-of-range defects.

the wafer at 95 °C for 10 min before a final development. The resist must be thin enough so that protons can pass through and reach the underlying silicon. Because of the resist thickness, the end of range of the protons in the silicon is modified according to the profile of the resist. Such spatial variations of the end of range result in 3D silicon microstructures which are curved in the vertical direction. Figures 6(*a*)–(*c*) show curved wires produced by irradiation with 1 MeV protons with a high line fluence of 5×10^{10} cm^{-1}, scanning lines on the surface, orthogonal to the resist lines. Because of the small, discontinuous resist step at the boundary, see figure 6(*d*) (inset), a high fluence was used to produce a thick wire width of 5 μm in figures 6(*a*)–(*c*) to ensure that the cores of the curved portion sufficiently overlapped with that of the bottom, flat portion. Many of the thinner curved wires of width of 1 μm, produced using a lower line fluence of 1×10^{10} cm^{-1}, shown in figure 6(*d*), have broken because of this discontinuous resist step. However, we believe that micrometer wide, curved lines can be successfully fabricated after optimizing the gray-scale mask patterning. After the fabrication process, the cores can be made narrower and smoother by oxidation. Figure 6(*c*) (inset) (ii) shows the core after oxidation at 900 °C for 4 h in air. If required, the silicon dioxide layer surrounding the core can be removed by a dilute HF solution.

3.4 Multilevel 3D wires

Multiple energy proton irradiation can be used to create localized defects at different depths within the silicon wafer to fabricate multilevel 3D structures, see process (iii) in figure 4. After anodization, the high defect core regions, produced by different proton energies, remain intact while the surrounding low defect regions between the cores form PSi. The line fluence of the highest proton energy is the only factor which influences the formation of the deepest cores. However, the layers of cores closer to the surface, formed by lower energy irradiations, are additionally influenced by the defects produced by irradiation of the deeper structures, which increases the resistivity along the path. This additional increment in resistivity should ideally be low enough to not significantly influence the formation of the PSi along the low-energy proton trajectory.

An array of two-level silicon wires running in orthogonal directions was fabricated with a period of 10 μm, figure 7(*a*). Line irradiations using 250 keV protons with line fluences of 1×10^{10} and 7×10^{10} cm^{-1} were used to fabricate shallow wires, while orthogonal line irradiations using 1 MeV protons with line fluences of 1×10^{10} and 5×10^{10} cm^{-1} were used to fabricate deeper wires, resulting in four different combinations of line fluence within the array, indicated as [c]–[f]. Supporting walls were formed by irradiation using a 2 MeV proton line fluence of 1.2×10^{12} cm^{-1}. After anodization and PSi removal, orthogonal free-standing lines at different depths

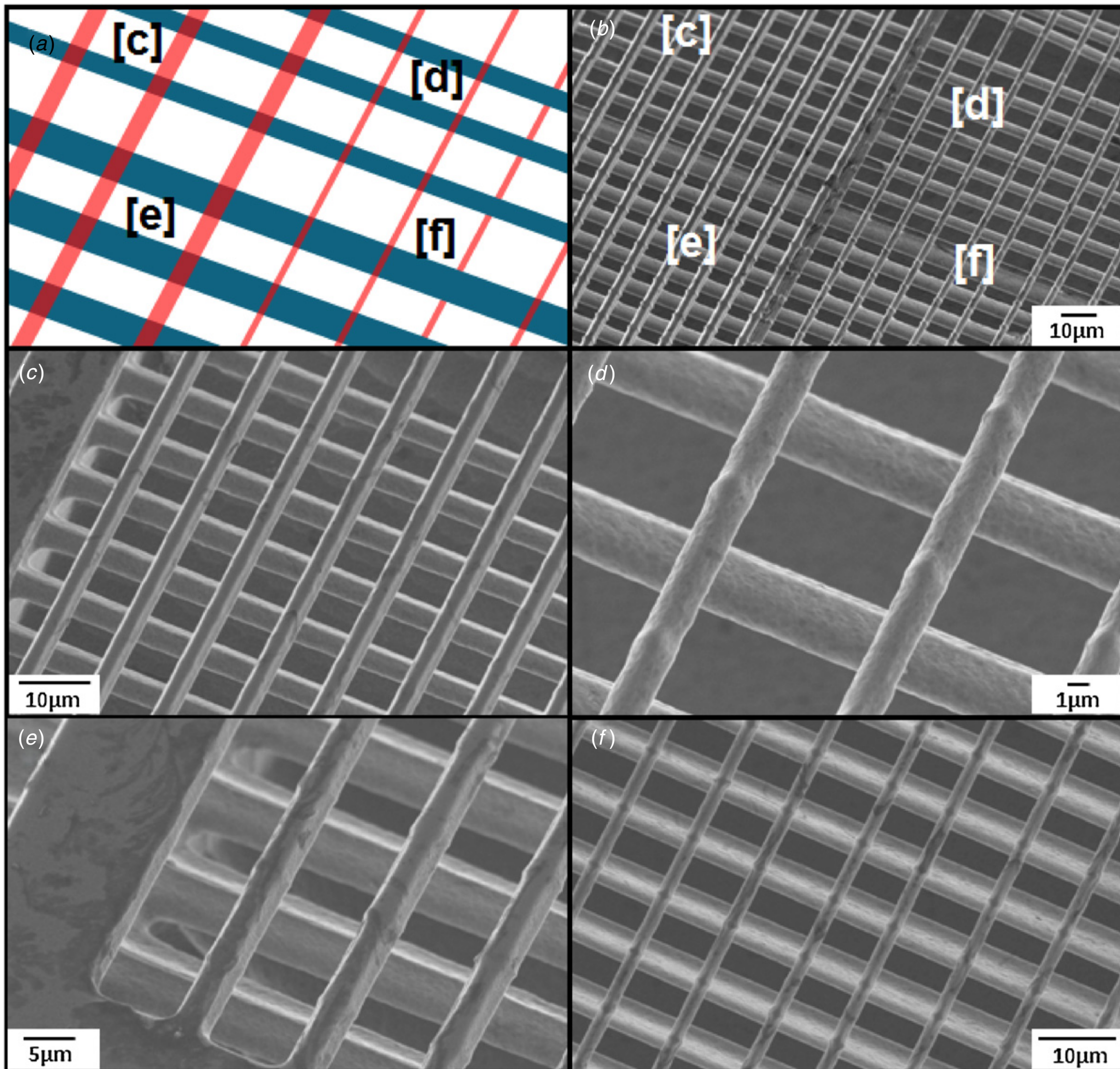

Figure 7. (*a*) A schematic of a two-level silicon wire array created with four irradiation combinations of line fluence and energy, where the thin/thick lines indicates a low/high fluence. Deep wires (shown in blue) are formed by irradiation with 1 MeV protons with a low line fluence of 1×10^{10} cm^{-1} in portions [c,d] and high line fluence of 5×10^{10} cm^{-1} in portions [e,f]. Shallow wires (shown in red) are formed by irradiation with 250 keV protons with a low line fluence of 1×10^{10} cm^{-1} in portions [d,f] and a high line fluence of 7×10^{10} cm^{-1} in portions [c,e]. (*b*) SEM showing the resultant 3D array of lines. (*c*)–(*f*) SEMs showing the close-up view of each combination, with same lettering as in figures 6(*a*) and (*b*).

were revealed, figure 7(*b*). Higher magnification SEMs of the four different line fluence combinations within this array are shown in figures 7(*c*)–(*f*), corresponding to the same letters indicated in figures 7(*a*) and (*b*). Wires irradiated at lower energy and lower line fluence are thinner due to the lower lateral scattering and smaller extent of the core region. Since both of these factors are important, the wire widths are similar in figure 6(*c*) even though they are formed with a factor of 7 difference in line fluence. Small bumps on the shallow wires at overlapping regions are observed in figures 7(*d*) and (*f*) owing to the additional defects produced by the orthogonal, high-energy irradiation, as discussed above. This effect is less pronounced in figures 6(*c*) and (*e*) where the shallow wires were irradiated with a line fluence high enough to act as an etch stop, so additional irradiation of the deeper layer has little effect.

A limitation of this process is that the ability to reduce the period is limited by the difficulty of forcing the anodization current through a more densely irradiated array. Hence, while figure 7 shows results obtained using a period of 10 μm, it becomes increasingly difficult to fabricate with smaller period. We can overcome this limitation by using a more heavily doped p-type wafer, such as that used in previous studies [24, 26–28]. The higher doping level makes it easier to leave sufficiently conducting paths for the hole current to flow through a more densely packed structure. Figure 8 shows a two-level array of parallel wires fabricated with the same process using 250 and 215 keV protons in 0.02 Ω cm silicon. The two levels of wires were irradiated at the same surface locations, each with a line fluence of 4×10^{10} cm^{-1} and a period of 3 μm. After anodization and removal of the porous silicon, free standing

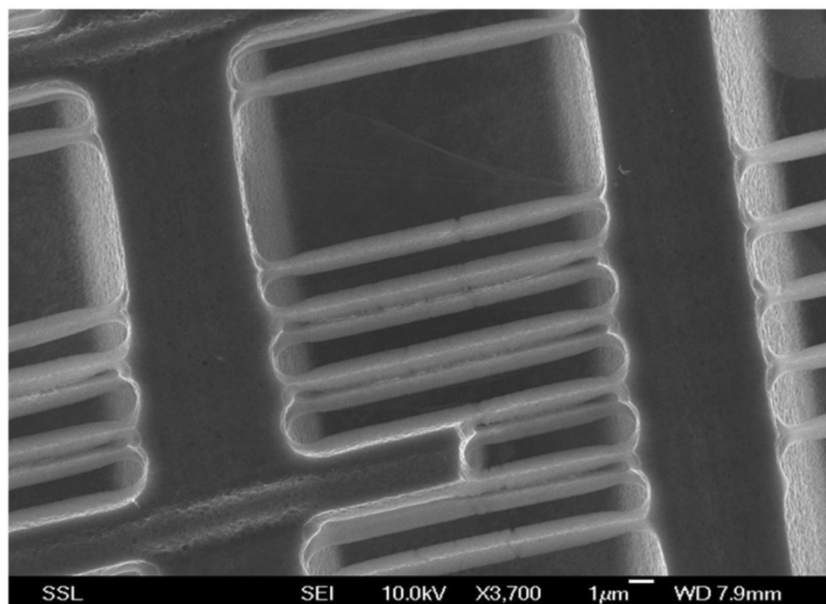

Figure 8. Two-level array of parallel wires fabricated using 0.02 Ω cm silicon wafer.

wires, supported by a wall fabricated at 1 MeV protons with a line fluence of 3×10^{12} cm^{-1}, are produced.

4. Conclusion

In conclusion, we demonstrate the ability of using localized defects created at the end of range of high-energy protons for machining complex 3D silicon structures within the bulk silicon after subsequent anodization and removing the PSi process. Curved 3D multilevel silicon structures may be fabricated using a gray-scale mask and multiple energy exposure. This is the only technique capable of doing so after a single-step etching. We believe that this process is an important development in fields such as silicon photonics and MEMS.

References

[1] Reed G T and Knights A P 2004 *Silicon Photonics: An Introduction* (New York: Wiley)
[2] Liu A, Jones R, Liao L, Samara-Rubio D, Rubin D, Cohen O, Nicolaescu R and Paniccia M 2004 A high-speed silicon optical modulator based on a metal-oxide-semiconductor capacitor *Nature* **427** 615–8
[3] Rong H, Jones R, Liu A, Cohen O, Hak D, Fang A and Paniccia M 2005 A continuous-wave Raman silicon laser *Nature* **433** 725–8
[4] Almeida V R, Barrios C A, Panepucci R R and Lipson M 2004 All-optical control of light on a silicon chip *Nature* **431** 1081–4
[5] Cleland A N and Roukes M L 1996 Fabrication of high frequency nanometer scale mechanical resonators from bulk Si crystals *Appl. Phys. Lett.* **69** 2653–5
[6] Fritz J, Baller M K, Lang H P, Rothuizen H, Vettiger P, Meyer E, Güntherodt H-J, Gerber C and Gimzewski J K 2000 Translating biomolecular recognition into nanomechanics *Science* **288** 316–8
[7] Craighead H G 2000 Nanoelectromechanical systems *Science* **290** 1532–5
[8] Lin S Y, Fleming J G, Hetherington D L, Smith B K, Biswas R, Ho K M, Sigalas M M, Zubrzycki W, Kurtz S R and Bur J 1998 A three-dimensional photonic crystal operating at infrared wavelengths *Nature* **394** 251–3
[9] Bustillo J M, Howe R T and Muller R S 1998 Surface micromachining for microelectromechanical systems *Proc. IEEE* **86** 1552–74
[10] Steve R and Robert P 2001 A review of focused ion beam applications in microsystem technology *J. Micromech. Microeng.* **11** 287
[11] Waits C M, Morgan B, Kastantin M and Ghodssi R 2005 Microfabrication of 3D silicon MEMS structures using gray-scale lithography and deep reactive ion etching *Sensors Actuators* A **119** 245–53
[12] Gantz K, Renaghan L and Agah M 2008 Development of a comprehensive model for RIE-lag-based three-dimensional microchannel fabrication *J. Micromech. Microeng.* **18** 025003
[13] Rao M P, Aimi M F and MacDonald N C 2004 Single-mask, three-dimensional microfabrication of high-aspect-ratio structures in bulk silicon using reactive ion etching lag and sacrificial oxidation *Appl. Phys. Lett.* **85** 6281–3
[14] Azimi S, Sandoughsaz A, Amirsolaimani B, Naghsh-Nilchi J and Mohajerzadeh S 2011 Three-dimensional etching of silicon substrates using a modified deep reactive ion etching technique *J. Micromech. Microeng.* **21** 074005
[15] Jeon J, Floresca H C and Kim M J 2010 Fabrication of complex three-dimensional nanostructures using focused ion beam and nanomanipulation *J. Vac. Sci. Technol.* B **28** 54
[16] Breese M B H, Jamieson D N and King P J C 1996 *Materials Analysis Using a Nuclear Microprobe* (New York: Wiley)
[17] Teo E J, Mangaiyarkarasi D, Breese M B H, Bettiol A A and Blackwood D J 2004 Controlled intensity emission from patterned porous silicon using focused proton beam irradiation *Appl. Phys. Lett.* **85** 4370
[18] Svensson B G, Mohadjeri B, Hallén A, Svensson J H and Corbett J W 1991 Divacancy acceptor levels in ion-irradiated silicon *Phys. Rev.* B **43** 2292–8
[19] Svensson B G, Jagadish C, Hallén A and Lalita J 1995 Point defects in MeV ion-implanted silicon studied by deep level transient spectroscopy *Nucl. Instrum. Methods Phys. Res.* B **106** 183–90
[20] Hallén A, Keskitalo N, Masszi F and Nagi V 1996 Lifetime in proton irradiated silicon *J. Appl. Phys.* **79** 3906

[21] Ziegler J F 2004 SRIM-2003 *Nucl. Instrum. Methods Phys. Res.* B **219–220** 1027–36
[22] Teo E J, Bettiol A A, Yang P, Breese M B H, Xiong B Q, Mashanovich G Z, Headley W R and Reed G T 2009 Fabrication of low-loss silicon-on-oxidized-porous-silicon strip waveguide using focused proton-beam irradiation *Opt. Lett.* **34** 659–61
[23] Teo E J, Xiong B Q, Ow Y S, Breese M B H and Bettiol A A 2009 Effects of oxide formation around core circumference of silicon-on-oxidized-porous-silicon strip waveguides *Opt. Lett.* **34** 3142–4
[24] Azimi S, Ow Y S and Breese M B H 2010 On the dependence of the surface roughness of electrochemically anodized silicon on ion irradiation fluence *Electrochem. Solid-State Lett.* **13** H382–H4
[25] Breese M B H, Champeaux F J T, Teo E J, Bettiol A A and Blackwood D J 2006 Hole transport through proton-irradiated p-type silicon wafers during electrochemical anodization *Phys. Rev.* B **73** 035428
[26] Ow Y S, Liang H D, Azimi S and Breese M B H 2011 Modification of porous silicon formation by varying the end of range of ion irradiation *Electrochem. Solid-State Lett.* **14** D45–7
[27] Ow Y S, Azimi S, Breese M B H, Teo E J and Mangaiyarkarasi D 2010 Effects of focused MeV ion beam irradiation on the roughness of electrochemically micromachined silicon surfaces *J. Vac. Sci. Technol.* B **28** 500–5
[28] Mangaiyarkarasi D, Breese M B H and Ow Y S 2008 Fabrication of three dimensional porous silicon distributed Bragg reflectors *Appl. Phys. Lett.* **93** 221905